metals

MDPI

Article

Aging Behaviour and Mechanical Performance of 18-Ni 300 Steel Processed by Selective Laser Melting

Riccardo Casati [1], Jannis N. Lemke [1], Ausonio Tuissi [2] and Maurizio Vedani [1,*]

[1] Dipartimento di Meccanica, Politecnico di Milano, Milano I-20156, Italy; riccardo.casati@polimi.it (R.C.); jannisnicolas.lemke@polimi.it (J.N.L.)

[2] Institute for Condensed Matter Chemistry and Technologies for Energy, CNR, Lecco I-23900, Italy; ausonio.tuissi@cnr.it

* Correspondence: maurizio.vedani@polimi.it; Tel.: +39-02-2399-8230

Academic Editor: Manoj Gupta

Received: 2 August 2016; Accepted: 5 September 2016; Published: 8 September 2016

Abstract: An 18-Ni 300 grade maraging steel was processed by selective laser melting and an investigation was carried out on microstructural and mechanical behaviour as a function of aging condition. Owing to the rapid cooling rate, the as-built alloy featured a full potential for precipitate strengthening, without the need of a solution treatment prior to aging. The amount of reversed austenite found in the microstructure increased after aging and revealed to depend on aging temperature and time. Similarly to the corresponding wrought counterpart, also in the selective laser-melted 18-Ni 300 alloy, aging promoted a dramatic increase in strength with respect to the as-built condition and a drop in tensile ductility. No systematic changes were found in tensile properties as a function of measured amount of austenite. It is proposed that the submicrometric structure and the phase distribution inherited by the rapid solidification condition brought by selective laser melting are such that changes in tensile strength and ductility are mainly governed by the effects brought by the strengthening precipitates, whereas the concurrent reversion of the γ-Fe phase in different amounts seems to play a minor role.

Keywords: selective laser melting; maraging steel; aging behaviour; reversed austenite

1. Introduction

Maraging steels are ultra-high strength Fe-Ni alloys developed mainly for aircraft, aerospace, and tooling applications. Their outstanding combination of strength and toughness results from the aging of a relatively soft martensite formed by cooling at moderate rates from the Ni-containing γ-Fe solid solution. Aging leads to the formation of strengthening precipitates. It is reported that in the 18-Ni 300 alloy and in similar grades, the Ni_3Ti phase (or more generally, Ni_3X where X = Ti, Mo, V, and W) readily form on short-term aging at low temperatures (400–450 °C), followed by Fe_2Mo or Fe_7Mo_6 precipitation [1–6]. Aging at temperatures exceeding 500 °C concurrently promotes the formation of austenite by a diffusion-controlled reaction, which is also favoured by the release of Ni into the matrix due to decomposition of Ni_3Ti phase [1,3,5–9].

Due to their good ductility and weldability, maraging steels recently attracted the attention as candidate alloys for additive manufacturing processes, such as selective laser melting (SLM). During SLM, layers of powder are selectively molten by a scanning laser beam and consolidated on top of each other. Fully dense parts can thus be generated featuring mechanical properties comparable to those of components processed by standard routes [10–12].

The mechanical behaviour of SLM parts is strongly affected by the refined microstructure inherited from fast cooling and by generation of small solidification faults [13–16]. Indeed, the localized melting process experienced during SLM is not yet fully understood. It is governed by laser beam

parameters, but also by surface morphology given by the pre-deposited layers and the stochastic particle distribution on the powder bed, as well as by the physical surface and bulk properties of the powder itself [17]. The solidification process and the resulting microstructure assume, therefore, an important role that still needs a deeper understanding and control. Concurrently, alloy optimization should consider these issues by deliberately promoting enhanced damage tolerance properties, especially when considering opportunities offered by tuning of alloy chemistry and the selection of post-SLM thermal treatments.

In wrought maraging parts requiring increased toughness, over-aged temper conditions are preferably selected in order to allow the formation of a controlled amount of austenite that remains stable even at room temperature. Such over-aging promotes softening and increases crack blunting effects [1]. However, this beneficial influence may be counterbalanced by matrix embrittlement when too coarse particles start acting as crack nucleation sites [8].

The present study is, therefore, aimed at investigating the mechanical behaviour of 18-Ni 300 maraging alloy samples produced by SLM as a function of specific microstructural conditions obtained by different thermal treatments. Analyses will be particularly focused on the possibility of improving the combination of strength and ductility by tailored aging treatments.

2. Materials and Methods

An 18-Ni 300 maraging alloy (1.2709) supplied by Sandvik Osprey LTD (Neath, UK) as gas-atomized powder was investigated. The alloy chemical composition is given in Table 1, while Figure 1 shows the general morphology of the batch of powder considered. From the particle size distribution obtained by laser diffraction analysis, an average particle size of 35 μm was obtained and it could be stated that 90% of the particles did not exceed the size of 54 μm.

Table 1. Chemical composition (weight fraction, %) of the investigated 18-Ni 300 steel powder.

Ni	Mo	Co	Ti	Al	Si
17.6	5.3	9.6	0.7	0.09	0.2

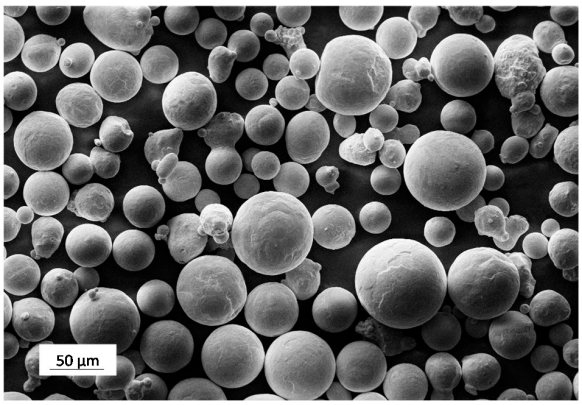

Figure 1. View of the 18-Ni 300 alloy powder investigated.

A Renishaw AM250 SLM system (Wotton-under-Edge, UK) was used to produce a set of samples consisting of horizontal and vertical bars (10 mm × 10 mm × 75 mm), as depicted in Figure 2. Melting of powder was performed under Ar atmosphere by a single mode fiber laser with a power of 200 W and an estimated beam diameter at a focal point of 75 μm. Laser melting was performed by discrete and partially overlapped spots exposed to the radiation for a fixed time (t) and their distance is called point distance (d_P). At the end of each scan line, the laser shifts to a partially overlapped adjacent line to scan the selected surface of the layer. The distance between adjacent scan lines is

defined as the hatch distance (d_H). Based on parameter optimization and manufacturer data, d_H, d_P, and t were set to 80 μm, 65 μm, and 80 μs, respectively. The thickness of each powder layer was set to 40 μm. Finally, samples were produced using a meander scanning strategy and by rotating the scanning direction by 67° after each layer.

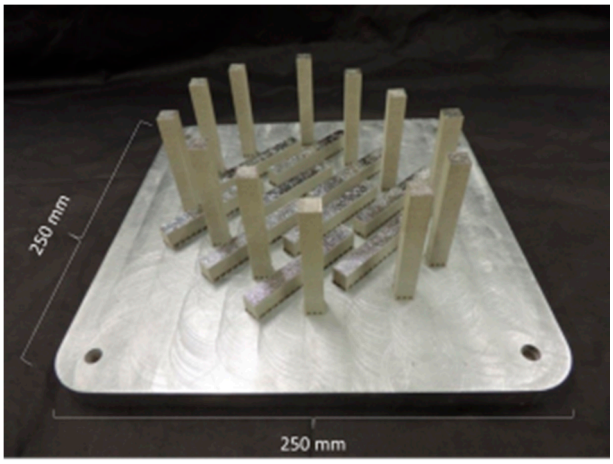

Figure 2. Geometry of SLM processed bars.

After removal from the steel base plate, the samples were sectioned and machined for further analyses. Microstructural observations were carried out by optical microscope (Leica Microsystems, Richmond Hill, ON, Canada), and by scanning electron microscope (SEM, Oberkochen, Germany) equipped with energy dispersive X-ray analysis (EDX, Oxford Instruments, Abingdon-on-Thames, UK) and electron back-scattered diffraction (EBSD, Oxford Instruments, Abingdon-on-Thames, UK) detectors. Samples were prepared by standard grinding and polishing followed by etching with Picral or modified Fry's reagent.

Aging response of the SLM samples was evaluated starting from samples both in the as-built condition and after a standard solution treatment, carried out at 815 °C for 30 min, followed by water quenching.

Differential scanning calorimetry (DSC, Labsys Setaram, Caluire, France) analyses were carried out on the as-built and on the solution treated samples (weight of about 50 mg) by temperature scans, at a rate of 20 °C/min in Ar atmosphere to assess precipitation sequence of strengthening phases. Isothermal aging curves (hardness vs. aging time at constant temperature) were then collected at 460, 490, 540, and 600 °C for times ranging from 10 min, up to 14 days. The evolution of hardness was followed by performing Vickers indentations with a load of 2 kg.

X-ray diffraction (XRD) patterns were collected using a X-Pert PRO (PANalitical, Almelo, The Netherlands) instrument equipped with a RTMS X'Celerator sensor. Cu Kα (k = 0.15418 nm) radiation was employed. Peaks identification and quantitative analysis of phases was performed by Rietveld method using Maud software. Samples for XRD were sectioned by diamond blade and polished down to 1 μm grit size, applying conventional metallographic methods. In order to avoid substantial structural modification, samples were carefully prepared by a very gentle and prolonged polishing stage.

Dog-bone tensile specimens having a gauge length of 20 mm and diameter of 4 mm were machined from bars treated according to different conditions investigated. In the present study only specimens built with their longitudinal axis oriented along the horizontal direction are considered. Tensile tests were performed at room temperature with a crosshead speed of 0.5 mm/min (corresponding to an initial strain rate of $4.2 \times 10^{-4} \cdot s^{-1}$) using a MTS Alliance RT/100 universal testing machine (MTS, Eden Prairie, MN, USA). At least three specimens for each condition were tested. Finally, fractographic analyses were carried out by SEM to identify the main fracture mechanisms.

3. Results

Figure 3 shows low-magnification views of the as built structure. The width and depth of the distinct laser tracks could be clearly identified after etching on lateral sections (Figure 3a). Views obtained from cross-sections taken perpendicularly to the build direction, hereafter referred to as top views, highlight the discontinuous nature of the melting process induced by the pulsed laser beam: distinct pools pertaining to different layers are visible on the same track (Figure 3b). High magnification micrographs taken by SEM reveal the expected cellular solidification structure and evidence of the epitaxial growth across different track boundaries, as shown in Figure 4.

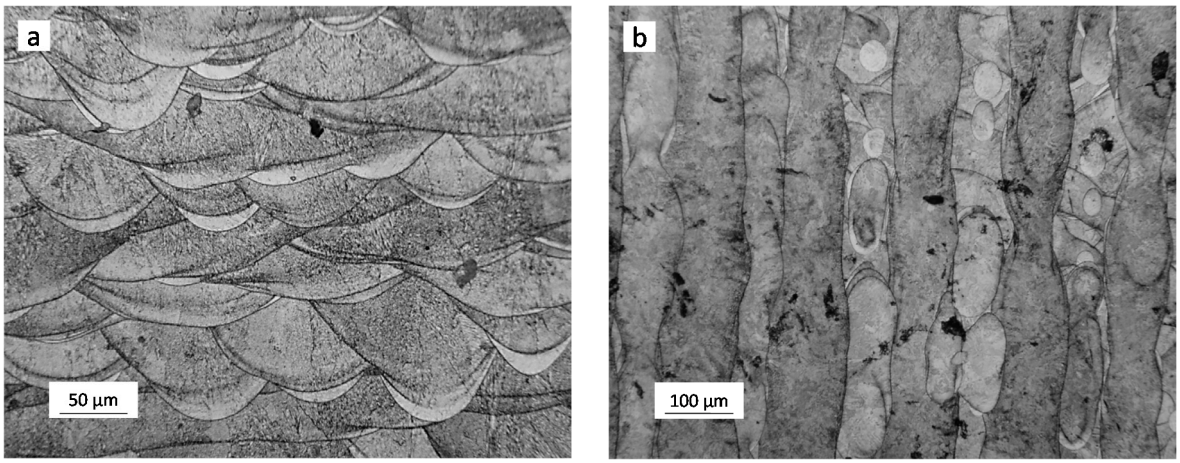

Figure 3. Optical images of the as built microstructure of the steel investigated. (**a**) Lateral view; and (**b**) top view.

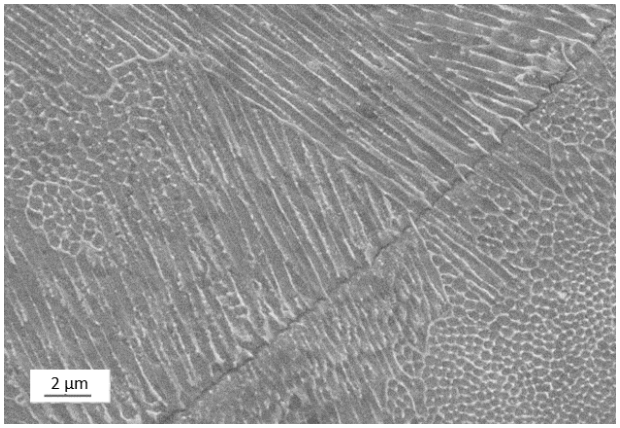

Figure 4. SEM image of the cellular solidification microstructure and epitaxial growth across a track boundary.

After solution treatment, the traces of solidification completely disappeared and the cellular structure was replaced by a martensitic structure, as depicted in Figure 5a. EBSD analyses showed that the martensitic structure was fairly coarse. According to literature, the detected microstructural features can be interpreted as massive martensite blocks or packets (depicted in Figure 5b by the EBSD orientation image), consisting of fine bundles of parallel, heavily dislocated laths [8,18]. Traces of reversed austenite (γ-Fe phase) were also revealed by phase maps based on crystallographic information. It can be stated that the γ-Fe phase is mainly located at boundaries of the martensite blocks (Figure 5c).

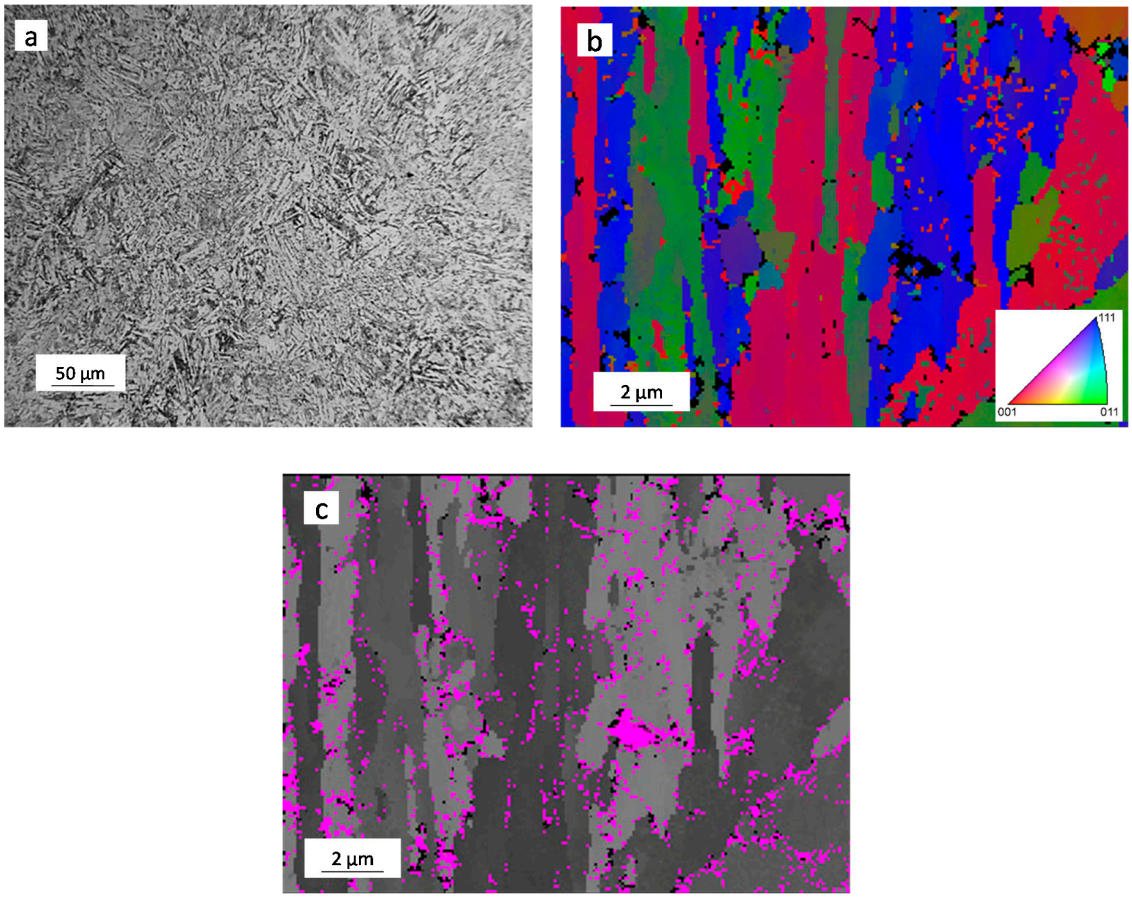

Figure 5. Representative micrographs of the solution treated sample, (**a**) revealed by optical microscopy; (**b**) EBSB orientation image; and (**c**) phase map highlighting γ-Fe phase (coloured in pink).

The aging behaviour of the SLM-treated 18-Ni 300 steel was first investigated by DSC analyses. A comparative study between samples cut from the as built and from solution treated materials, shown in Figure 6a, allowed to state that the aging sequence for these two tempers was substantially equivalent. Both DSC curves exhibited four peaks. The first exothermic peak (peak #1) is believed to be produced by the formation of carbide or coherent precipitation zones, whereas the second exothermic peak (peak #2) is usually associated in the literature to the formation of the main strengthening precipitates, namely the Ni_3Ti phase followed by Fe_2Mo or Fe_7Mo_6 [1–4,19]. The endothermic peaks (peaks #3 and #4) are likely due to the austenite reversion and to the dissolution of precipitates [4,19].

Isothermal aging treatments were carried out at selected temperatures on both the as-built and the solution-treated samples to evaluate possible differences in the achievable strength. In Figure 6b the hardness evolution during aging at 490 °C is reported. The solution annealing leads to a hardness drop from 371 HV to 279 HV which is believed to be due to stress relieving effects and to slight coarsening of the microstructure. However, this gap in hardness is readily bridged after only 30 min of aging. Thereafter, the hardness of the two samples remains comparable for all of the aging times considered here, in full agreement with observations derived from the DSC results.

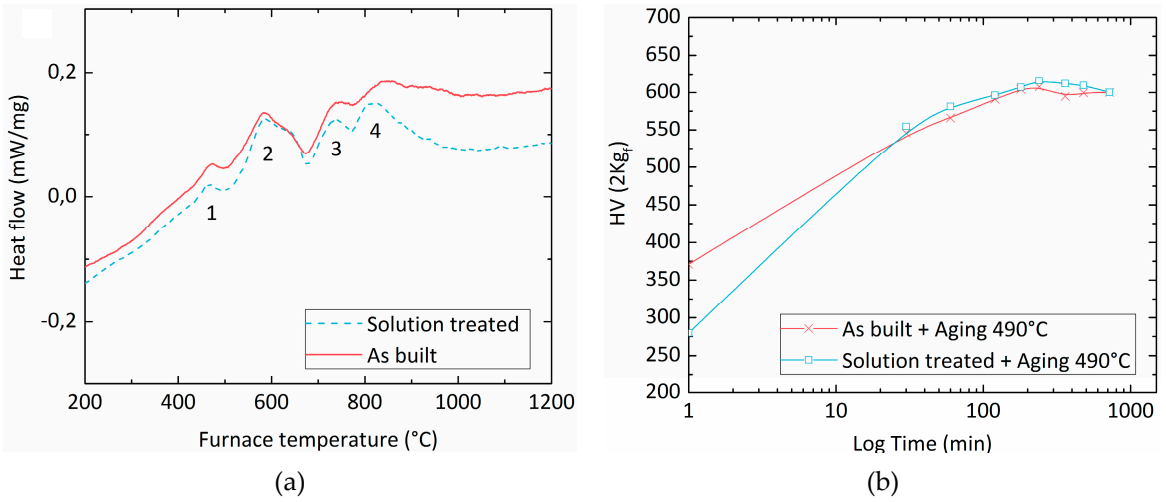

Figure 6. DSC scans at a heating rate of 20 °C/min comparing the aging behaviour of as-built and solution-treated samples (**a**). Hardness evolution of the two corresponding samples during isothermal holding at 490 °C (**b**).

Isothermal aging curves collected starting from as built samples are depicted in Figure 7. The expected strengthening trend as a function of aging time is revealed for all of the investigated temperatures. Peak aging times can be identified as: 10 min, 1 h, 4 h, and 8 h for the temperatures of 600, 540, 490, and 460 °C, respectively. Marked over-aging effects (i.e., sharp hardness drop once the peak hardness time is exceeded) were observed for the highest temperature levels (540 and 600 °C), while over-aging at 460 and 490 °C only led to moderate loss in hardness.

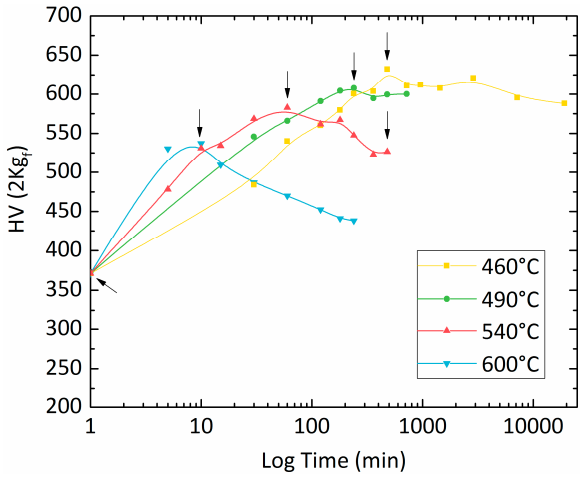

Figure 7. Vickers hardness vs. aging time of as-built samples collected at different aging temperatures. Samples selected for further analyses are marked with arrows.

Based on the above results, further analyses on mechanical behaviour were focussed on samples aged to their peak hardness conditions at the different aging temperatures. An additional condition was selected by over-aging for 8 h at 540 °C. This temper allows comparisons to be made with a 600 °C peak-aged sample (comparable hardness but different aging times) and a 460 °C peak-aged sample (same aging time but different resulting hardness).

Since holding at temperatures exceeding 500 °C is expected to promote extensive reversion of martensite into austenite in wrought maraging steels [1,3,5–9], XRD and microstructural analyses were carried out to asses phase balance in the investigated samples. Figure 8 summarizes the XRD spectra

acquired from samples treated according to different aging conditions, while quantitative evaluation of the γ-Fe phase fraction is reported in Table 2. A marked increase in austenite content is induced by aging. Further slight decomposition of martensite could be achieved by also increasing the aging temperature and by extensively over-aging the samples (e.g., aging 8 h at 540 °C).

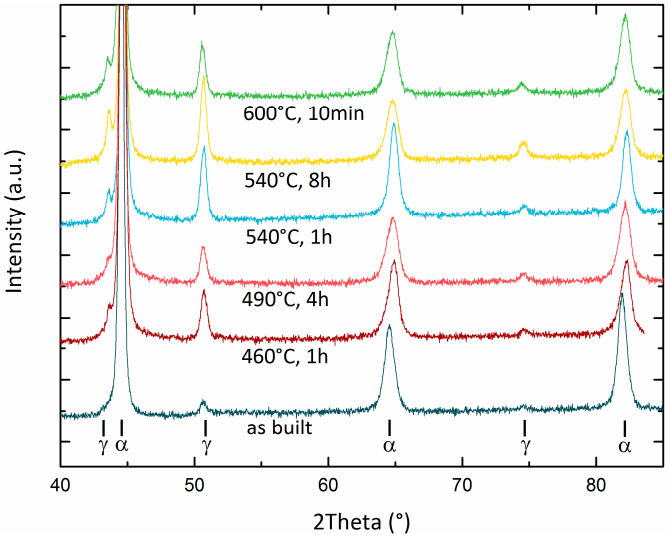

Figure 8. XRD spectra of the 18-Ni 300 steel as a function of aging condition.

Table 2. Austenite (γ-Fe) fraction and corresponding tensile properties as a function of aging temper. Standard deviation of data is also given in brackets.

Condition	γ-Fe Fraction (%)	YS (MPa)	UTS (MPa)	Elongation (%)
as built	11.38 (1.02)	914.9 (12.5)	1187.6 (10.4)	6.14 (1.33)
460 °C 8 h	15.55 (0.73)	1956.8 (43.3)	2017.1 (57.7)	1.51 (0.20)
490 °C 4 h	16.12 (0.57)	1793.3 (96.5)	1814.6 (95.1)	1.20 (0.13)
540 °C 1 h	17.17 (0.68)	1870.3 (53.8)	1956.9 (54.2)	2.07 (0.32)
540 °C 8 h	21.30 (0.77)	1545.9 (103.1)	1655.5 (87.5)	1.77 (0.05)
600 °C 10 min	17.15 (0.68)	1557.2 (140.4)	1659.1 (119.4)	1.60 (0.09)

The measured modifications also reflected into changes of the observed microstructure. In Figure 9, a collection of representative SEM micrographs is given. On aging, an increased amount of austenite (bright constituent in Figure 9) decorating cell boundaries became visible while over-aging additionally promoted precipitation of austenite at intragranular sites (Figure 9d,f).

Table 2 also summarizes the main average data collected by room temperature tensile tests. Low-temperature aging promotes a dramatic increase in strength over the as built condition. The yield strength improved from 915 MPa of the as built steel to 1957 and 1793 MPa for samples peak-aged at 460 and 490 °C, respectively. Conversely, fracture elongation underwent a drop from 6.1% to 1.5% and 1.2% for the same materials. The ultimate tensile strength (UTS) and 0.2% yield strength (YS) given in Table 2 for standard peak aging at 490 °C are substantially consistent with specifications for wrought products (e.g., ASTM A 538, AMS 6514, and MIL-S-46850 standards) and in good agreement with literature data on SLMed type 300 maraging steel [10]. Tensile ductility values between 1.2% and 2.1% were recorded from tests, irrespective of aging temperature and resulting austenite fraction. The poor fracture elongation of SLMed specimens after peak aging is also consistent with literature [10]. Figure 10 reports the tensile curves of samples peak aged at 460 °C and of as built samples to highlight the dramatic differences in tensile behaviour between these two conditions.

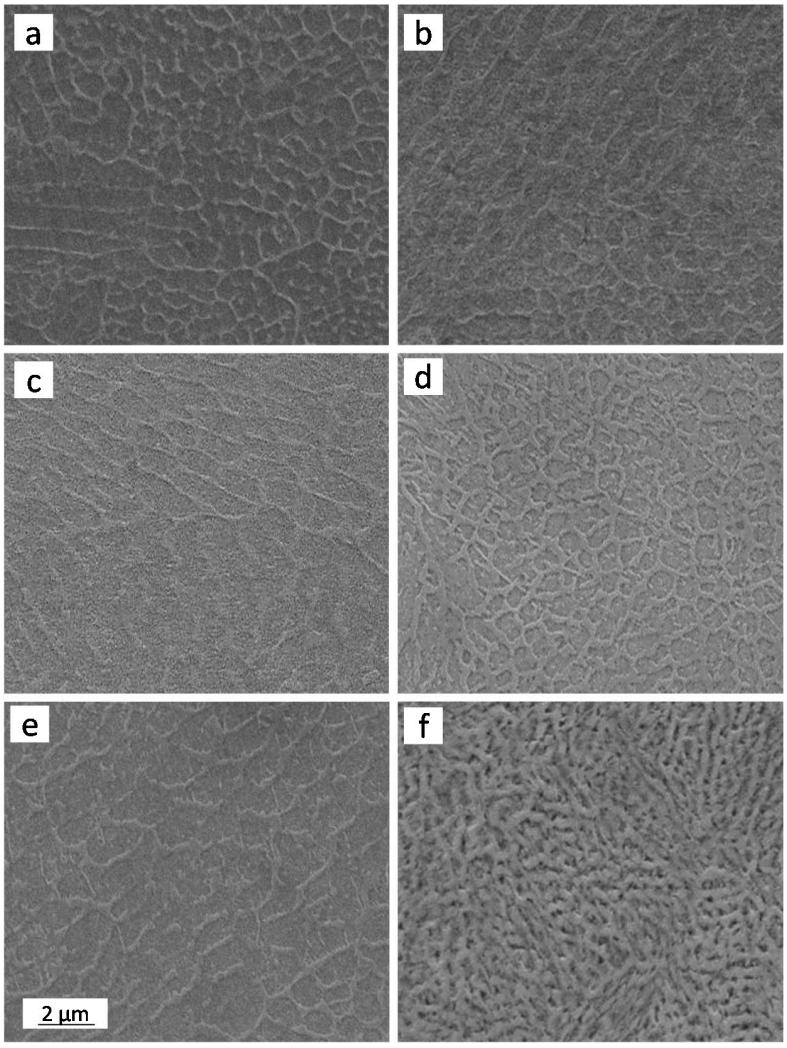

Figure 9. Microstructure (top view) of SLM processed 18-Ni 300 alloy samples aged at different temperatures and times. (**a**) 460 °C 8 h; (**b**) 490 °C 4 h; (**c**) 540 °C 1 h; (**d**) 540 °C 8 h; (**e**) 600 °C 10 min; and (**f**) 600 °C 4 h.

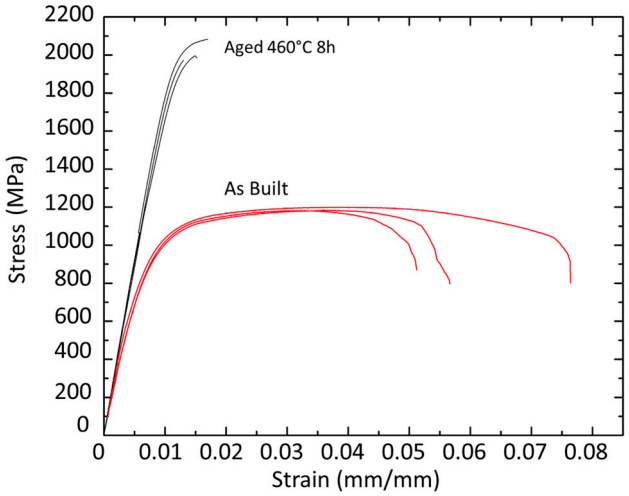

Figure 10. Tensile curves of as built and peak aged 18-Ni 300 steel.

Analysis of the fracture surfaces of broken tensile specimens clearly showed that fracture of the as-built samples was based on a ductile-type failure mechanism consisting in void nucleation, growth and their coalescence. Larger voids mainly originated from pre-existing defects, such as unmelted powder particles (see spherical particles in Figure 11a), splats (larger remelted particles that are blown away from the molten pool and are then engulfed into the following layers), cavities originated by incomplete melting between adjacent tracks. Peak aged samples (Figure 11b) featured similar fracture nucleation sites but the development of cracks was mainly ruled by a quasi-cleavage decohesion mechanism, presumably across the martensite blocks (compare Figures 5 and 11b).

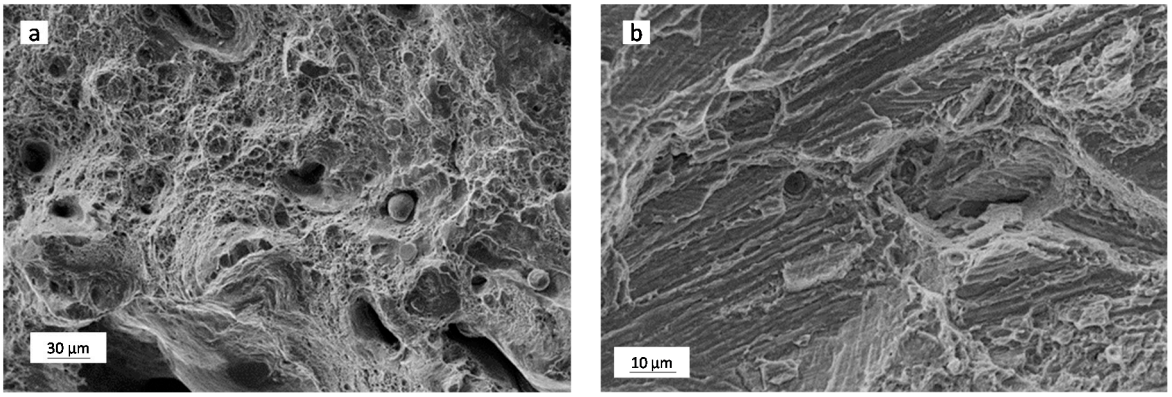

Figure 11. Fracture surfaces of broken tensile specimens: (**a**) as-built sample; and (**b**) 460 °C peak-aged sample.

Additional information about development of cracks under tension can be drawn by observing longitudinally-sectioned specimens close to the fracture line, as shown in Figure 12. The low magnification image (Figure 12a) allows one to highlight the growth of relatively large cracks starting from boundaries of adjacent laser tracks, whereas, from higher magnification views (Figure 12b), it can be suggested that the presence of reversed austenite located at boundaries of cells does not play a crucial role on fracture process.

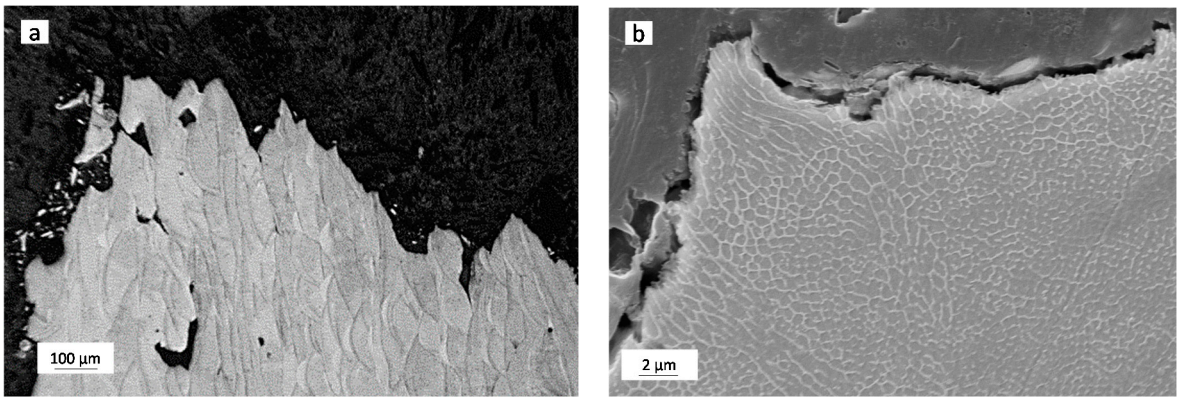

Figure 12. Low-magnification views of longitudinally-sectioned broken tensile specimens close to the fracture line. (**a**) As-built sample, optical image; and (**b**) 460 °C peak-aged sample, SEM image.

4. Discussion

Wrought maraging steels are usually aged after a solution treatment carried out at high temperature to homogenize the microstructure inherited from previous operations and to fully transform it into martensite on cooling. Even though it is stated that martensite can form even after moderate cooling rates, in published research works either water cooling [2,4] or air cooling [5,8]

were adopted. From the present results (DSC scans and evolution of hardness during isothermal aging) it can be inferred that the solidification and cooling rates induced by SLM processing are fast enough to preserve the full aging potential of the 18-Ni 300 maraging alloy without any need to perform an additional post-SLM solution treatment. This result is in full agreement with the research work published by Jägle and coauthors [6]. By atom probe tomography, these researchers were able to show that, in a Co-containing maraging steel similar to the present alloy, no precipitates or clusters of atoms were present in the SLM as-built state, even considering that each layer had been subjected to significant reheating during the layer-by-layer manufacturing process.

Further literature referred to welding of a wrought 18-Ni 250 grade maraging steel [18] also reports that, in the absence of high-temperature homogenizing treatments, the as-welded microstructure might contain segregation of Mo and Ti at cell boundaries. Especially, Mo can enhance the reversion rate of martensite into austenite on aging due to early formation of Fe_2Mo, resulting in local enrichment in Ni of the matrix. Molinari et al. [19] also claimed that aging and austenite reversion is accelerated by enhanced density of structural defects in maraging steel processed by spark plasma sintering. A similar effect is expected to be active also in the rapidly solidified samples here investigated. Microstructure observations (Figure 9) confirmed that austenite reversion on aging first occurred at cell boundaries and only on over-aging (8 h at 540 °C and 4 h at 600 °C) intracellular austenite could appear.

Reversion of austenite during aging in wrought alloys can be used to tune ductility and fracture toughness. Viswanathan and co-workers [8], by investigating a wrought 18-Ni 350 maraging steel, stated that reversed austenite causes a decrease in yield strength and ultimate tensile strength but it is beneficial to tensile ductility and impact toughness in the initial stages of over-aging. The same authors also investigated the morphology of reversed austenite formed at different stages of over-aging. It is to remark that in the wrought alloy, austenite appeared both as submicrometric-size precipitates at boundaries of martensite blocks and as much coarser intragranular pockets, around five micrometres in size.

In the SLMed samples of the present investigation, retained austenite was already found in as-built samples and further precipitated, mainly at boundaries of cells, in a very dispersed form on aging. It can be reasonably supposed that their tiny size and fine dispersion, as opposed to the micrometric pocket-like phases found in wrought alloys, is such to avoid a substantial toughening action as crack arrester phase.

Finally, it is to remark that the austenite reversion was stimulated in the present investigation by prolonged aging treatments (i.e., over-aging). However, the progression of aging generates a number of combined effects that have to be carefully analysed before drawing any conclusion about the present results. Aging mainly promotes: (i) the reversion of martensite into softer austenite; (ii) the formation of strengthening precipitates; (iii) the coarsening of precipitates and embrittelement of alloy on over-aging.

The combined effects of age hardening and softening induced by formation of reversed austenite in the investigated SLMed alloy can be better analysed by replotting the full dataset of tensile properties, as shown in Figure 13. The inverse relation between yield strength and tensile ductility is readily observed in Figure 13a where clustering of the data points into two distinct regions is also noticed. A first group of data referred to aged samples is visible on the top left corner of the plot, while the three data points pertaining to as built samples are displayed on the right side of the plot, showing moderate strength levels, but higher tensile ductility.

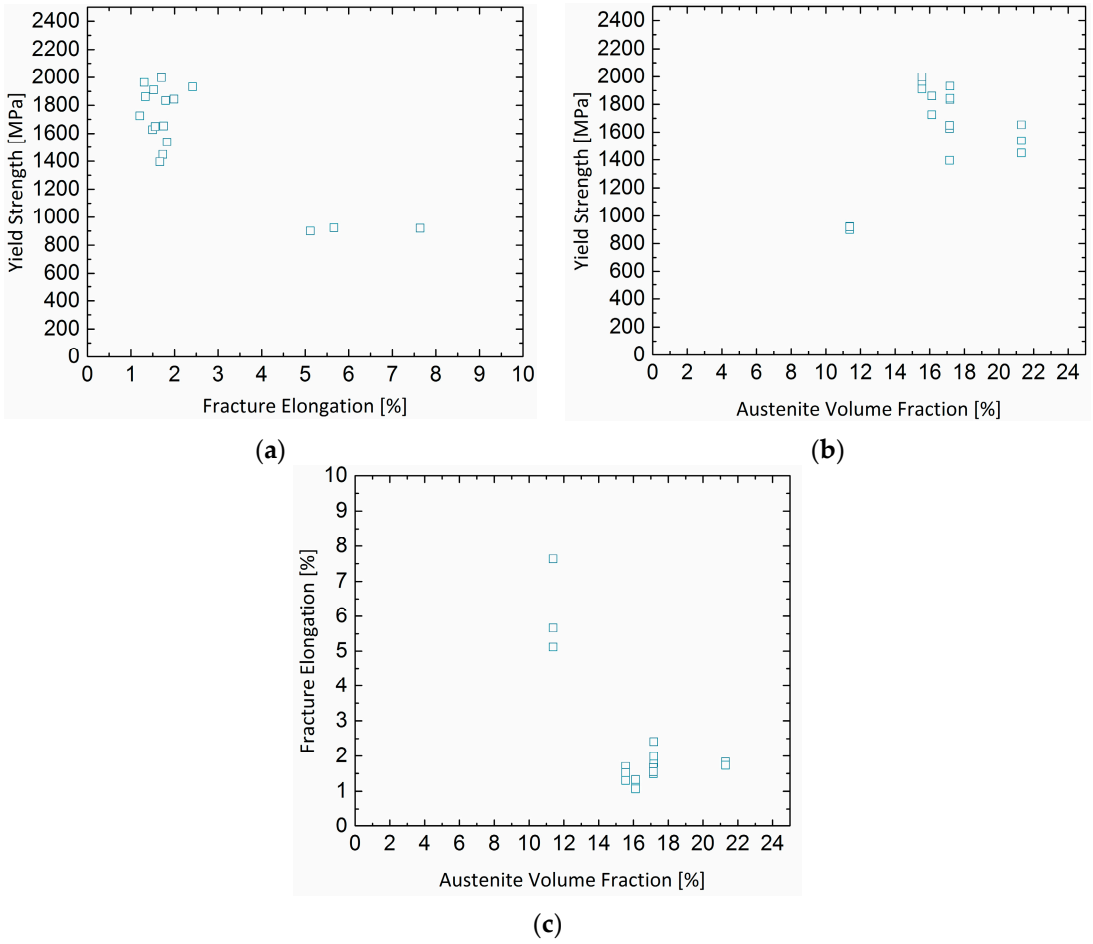

Figure 13. Relation between 0.2% yield strength, tensile elongation at fracture, and austenite volume fraction for the SLM processed 18-Ni 300 steel.

Both fracture elongation and yield strength can then be independently plotted as a function of austenite volume fraction, as depicted in Figure 13b,c, respectively. These figures highlight an unexpected trend considering that austenite can act, in principle, as a soft and more ductile constituent in steel microstructures. These results remark an important difference brought by the peculiar microstructural features generated by SLM processing with respect to the microstructure found in wrought products. Indeed, the highest yield strength and lower tensile elongation found for peak-aged samples (that also feature higher fractions of austenite) over the as-built condition are believed to be mainly due to the overwhelming effect of strengthening precipitates, whereas the concurrent reversion of the γ-Fe phase seems to play a minor role.

5. Conclusions

A study was undertaken to investigate the effects of selective laser melting on 18-Ni 300 maraging steel microstructure and mechanical behaviour. The main conclusions can be summarized as follows:

A submicrometric cellular microstructure was detected in the as-built samples. Evidence of epitaxial growth across different laser tracks was revealed. After high-temperature solution annealing, the traces of solidification were lost and the cellular structure was replaced by fairly coarse martensite blocks. Small fraction of austenite were preferentially located at block boundaries.

A comparison about the aging behaviour of the as-built and the solution-treated alloy revealed that the precipitation sequence during aging and hardness evolution are substantially equivalent.

X-ray diffraction and microstructural observation showed that aging also promotes a partial reversion of martensite into austenite. A shift to higher aging temperatures and over-aging further increased the amount of γ-Fe phase.

Different aging temperatures were selected to evaluate tensile performance of the peak-aged and over-aged samples as a function of the amount of reversed austenite. The results showed that aging promotes a dramatic increase in strength over the as built condition, but also a drop in tensile ductility. Among aged and over-aged samples, no systematic changes were found in tensile properties as a function of measured austenite.

It is suggested that, as opposed to the trend expected in corresponding wrought maraging alloys, the submicrometric structure inherited by the rapid solidification condition brought by selective laser melting are such that changes in tensile strength and ductility are mainly governed by the effects given by the strengthening precipitates, whereas the concurrent reversion of the γ-Fe phase seems to play a minor role.

Acknowledgments: The financial support of Regione Lombardia (Bando Creatività Linea 2, AddMe.Lab project) is acknowledged.

Author Contributions: R.C. and J.N.L. performed the experiments. A.T. contributed to XRD analysis and discussion of results. R.C. and M.V. wrote the paper. M.V. supervised the project.

Conflicts of Interest: The authors declare no conflicts of interest.

References

1. Pardal, J.M.; Tavares, S.S.M.; Terra, V.F.; da Silva, M.R.; dos Santos, D.R. Modeling of precipitation hardening during the aging and overaging of 18Ni-Co-Mo-Ti maraging 300 steel. *J. Alloy. Compd.* **2015**, *393*, 109–113. [CrossRef]
2. Sha, W.; Cerezo, A.; Smith, G.D.W. Phase Chemistry and Precipitation Reactions in Maraging Steels: Part I. Introduction and Study of Co-Containing C-300 Steel. *Metall. Trans. A* **1993**, *24A*, 1221–1232. [CrossRef]
3. Pardal, J.M.; Tavares, S.S.M.; Fonseca, M.P.C.; Abreu, H.F.G.; Silva, J.J.M. Study of the austenite quantification by X-ray diffraction in the 18Ni-Co-Mo-Ti maraging 300 steel. *J. Mater. Sci.* **2006**, *41*, 2301–2307. [CrossRef]
4. Guo, Z.; Sha, W.; Li, D. Quantification of phase transformation kinetics of 18 wt. % Ni C250 maraging steel. *Mater. Sci. Eng. A* **2004**, *373*, 10–20. [CrossRef]
5. Tewari, R.; Mazumder, S.; Batra, I.S.; Dey, G.K.; Banerjee, S. Precipitation in 18 wt. % maraging steel of grade 350. *Acta Mater.* **2000**, *48*, 1187–1200. [CrossRef]
6. Jägle, E.A.; Choi, P.P.; van Humbeeck, J.; Raabe, D. Precipitation and austenite reversion behavior of a maraging steel produced by selective laser melting. *J. Mater. Res.* **2014**, *29*, 2072–2079. [CrossRef]
7. Li, X.; Yin, Z. Reverted austenite during aging in 18Ni (350) maraging steel. *Mater. Lett.* **1995**, *24*, 239–242. [CrossRef]
8. Viswanathan, U.K.; Dey, G.K.; Sethumadhavan, V. Effects of austenite reversion during overageing on the mechanical properties of 18 Ni (350) maraging steel. *Mater. Sci. Eng. A* **2005**, *398*, 367–372. [CrossRef]
9. Tavares, S.S.M.; Abreu, H.F.G.; Neto, J.M.; da Silva, M.R.; Popa, I. A thermomagnetic study of the martensite-austenite phase transition in the maraging 350 steel. *J. Alloy. Compd.* **2003**, *358*, 152–156. [CrossRef]
10. Kempen, K.; Yasa, E.; Thijs, L.; Kruth, J.-P.; van Humbeeck, J. Microstructure and mechanical properties of Selective Laser Melted 18Ni-300 steel. *Phys. Proc.* **2011**, *12*, 255–263. [CrossRef]
11. Casalino, G.; Campanelli, S.L.; Contuzzi, N.; Ludovico, A.D. Experimental investigation and statistical optimization of the selective laser melting process of a maraging steel. *Opt. Laser Technol.* **2015**, *65*, 151–158. [CrossRef]
12. Croccolo, D.; de Agostinis, M.; Fini, S.; Olmi, G.; Vranic, A.; Ciric-Kostic, S. Influence of the build orientation on the fatigue strength of EOS maraging steel produced by additive metal machine. *Fat. Fract. Eng. Mater. Struct.* **2016**. [CrossRef]
13. Murr, L.E.; Martinez, E.; Amato, K.N.; Gaytan, S.M.; Hernandez, J.; Ramirez, D.A.; Shindo, P.W.; Medina, F.; Wicker, R.B. Fabrication of metal and alloy components by additive manufacturing: Examples of 3D materials science. *J. Mater. Res. Technol.* **2012**, *1*, 42–54. [CrossRef]

14. Frazier, W.E. Metal additive manufacturing: A review. *J. Mater. Eng. Perform.* **2014**, *23*, 1917–1928. [CrossRef]
15. Gu, D.D.; Meiners, W.; Wissenbach, K.; Poprawe, R. Laser additive manufacturing of metallic components: Materials, processes and mechanisms. *Int. Mater. Rev.* **2012**, *57*, 133–164. [CrossRef]
16. Casati, R.; Lemke, J.; Vedani, M. Microstructure and Fracture Behavior of 316L Austenitic Stainless Steel Produced by Selective Laser Melting. *J. Mater. Sci. Technol.* **2016**. [CrossRef]
17. Bauereiß, A.; Scharowsky, T.; Körner, C. Defect generation and propagation mechanism during additive manufacturing by selective laser melting. *J. Mater. Process. Technol.* **2014**, *214*, 2522–2528. [CrossRef]
18. Shamantha, C.R.; Narayanan, R.; Iyer, K.J.L.; Radhakrishnan, V.M.; Seshadri, S.K.; Sundararajan, S.; Sundaresan, S. Microstructural changes during welding and subsequent heat treatment of 18Ni (250-grade) maraging steel. *Mater. Sci. Eng.* **2000**, *A287*, 43–51. [CrossRef]
19. Menapace, C.; Lonardelli, I.; Molinari, A. Phase transformation in a nanostructured M300 maraging steel obtained by SPS of mechanically alloyed powders. *J. Therm. Anal. Calorim.* **2010**, *101*, 815–821. [CrossRef]